ACS APPLIED MATERIALS & INTERFACES

Research Article

www.acsami.org

Facile and Efficient Route to Polyimide-TiO_2 Nanocomposite Coating onto Carbon Fiber

Shuqing He,[†,‡] Chunxiang Lu,*[,†] and Shouchun Zhang[†]

[†]National Engineering Laboratory for Carbon Fiber Technology, Institute of Coal Chemistry, Chinese Academy of Sciences, Taiyuan 030001, P.R. China

[‡]Graduate University of Chinese Academy of Sciences, Beijing 100049, P.R. China

ABSTRACT: Polyamic acid-TiO_2 hybrid colloid emulsion with an average particle size of 200 nm was formed by dispersing nano-TiO_2 into polyamic acid colloidal emulsion. The polyimide-TiO_2 nanocomposite was coated onto carbon fiber by electrophoretic deposition. The primary properties of polyamic acid-TiO_2 hybrid colloid emulsion and polyimide-TiO_2 nanocomposite coating onto carbon fiber were characterized using laser scattering, ZetaPlus particle sizing, transmission electron microscopy, field-emission scanning electron microscope, Fourier transforms infrared spectroscopy, and X-ray Diffraction analysis. The results indicated that the small amount of nano-TiO_2 would be effectively dispersed in polyamic acid colloidal particles. The polyimide-TiO_2 hybrid nanocomposite coating carbon fiber sheet displayed an excellent photodegradation performance of methyl orange, which could be degraded more than 70 wt % after 10 cycles.

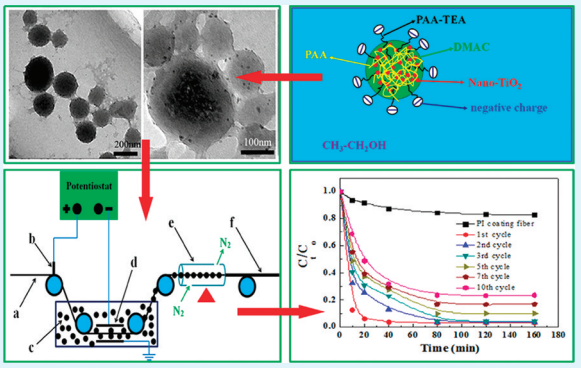

KEYWORDS: *electrophoretic deposition, hybrid colloid emulsion, nanocomposite coating, carbon fiber*

1. INTRODUCTION

Recently, semiconductor photocatalysts have attracted much research attention because of their applications to environmental purification.[1,2] Among these photocatalysts, TiO_2 appears to be the most promising and suitable material because of its strong oxidizing ability, nontoxicity and long-term stability.[3,4] However, traditional nano-TiO_2 powders need to be dispersed into the water, so it is impossible to use them to purify rivers or lakes because of it is difficult to recover and will bring about secondary pollution. Porous carbon has been proved as an effective support for TiO_2 in the removal of the pollutants combining adsorption and photocatalytic processes.[5−7] In general, porous carbons are in the forms of granules and powder, which inhibit its scale application and recovery catalyst from water.

Carbon fiber sheet with higher specific strength, high stiffness and chemical stability are widely used as reinforcement in composite materials, such as carbon fiber reinforced cement, plastics, and carbon−carbon composite.[8−10] Now, carbon fiber is utilized as a supporter of photocatalysis[11] and microwave absorption.[12−14] It is very difficult to support metal oxides onto carbon fiber because of the weak surface chemical interaction. When TiO_2 nanotube or ZnO nanowire were grown on carbon fiber sheets under hydrothermal method, it showed efficient photocatalytic activity under weak UV light irradiation and high interfacial strength, respectively.[11,15] However, it is complex and difficult to carry a continuous production. Therefore, it is necessary to seek a new process or method to combine TiO_2 on carbon fiber surface.

Compared with the various apporaches for modifying the carbon fiber surface, such as grafting coupling agents,[16] electrochemical treatment,[17] and growing carbon nanotube,[18] coating is a simple and effective method for carbon fiber surface modification. Organic−inorganic hybrid coating technology is being developed to improve carbon fiber composite functional performance in extreme environment due to its advantages of inorganic material (e.g., inertness, UV resistance, and thermal stability) and the organic polymer (e.g., flexibility, toughness, and ductility) with most active areas.[19−21] For example, TiO_2 has been deposited on glass fibers with a partial epoxy layer coating from a solution containing TiO_2 nanoparticles (less than 25% glass surface covered by TiO_2 nanoparticles).[22] Polyimide is a preferable organic matrix candidate in the manufacture of advanced composite materials because of its unusual good thermal stability, high mechanical strength, and chemical inertness.[23−25] Moreover, polyimide-TiO_2 hybrid materials using sol−gel process have been considered as suitable materials for preparing advanced hybrid composite coating that have potential applications in the microelectronics, aircraft industries, and films areas.[26−28] To get a uniform and continuous coating, electrophoretic deposition (EPD) is a convenient and widely used method to deposit electrically charged colloidal particles onto conductive substrate.[29,30]

Received: September 13, 2011
Accepted: November 14, 2011
Published: November 14, 2011

In the present work, polyamic acid (PAA)-TiO_2 hybrid colloid emulsion and polyimide (PI)-TiO_2 nanocomposite coating onto carbon fiber were obtained by EPD. The properties of PAA-TiO_2 hybrid colloidal particles and the morphology and chemical and physical properties of PI-TiO_2 nanocomposite coating were investigated and compared. The possible formation mechanism of PAA-TiO_2 hybrid colloidal particles and the photocatalytic activity of carbon fiber coating PI-TiO_2 nanocomposite sheet were analyzed and discussed.

2. EXPERIMENTAL SECTION

Materials and Chemicals. Carbon fiber (T300-3k, PAN-based) was purchased from Toray Industries, Inc. (Japan) and its special properties was shown in Table 1. Pyromellitic dianhydride (PMDA, ≥ 98.5%), 4, 4′-oxidianiline (ODA, ≥ 98.0%), N,N-dimethylacetamide (DMAC, AR), triethylamine (TEA, AR), methanol (AR), and methyl orange were purchased from Sinopharm Chemical Reagent Co, Ltd. (SCRC, China). ODA, DMAC, and TEA were recrystallized in ethyl acetate or distillation prior to use, respectively. Titanium dioxide (≥99.9%, anatase phase, 150 m^2/g of surface area and 15 nm of particle size) used in this study was purchased from Nanjing High Technology Nano Material Co., Ltd. China.

Table 1. Physical Properties of Carbon Fiber (T300-3K)

carbon fiber	tensile strength (GPa)	tensile modulus (GPa)	density (g/cm^3)	failure strain (%)	diameter (μm)
T300-3K	3.90 ± 0.10	230 ± 2	1.70 ± 0.01	≥1.5	7.0 ± 0.1

PAA-TiO_2 Hybrid Colloid Emulsion. A typical synthesis process of PAA solution was shown in Chart 1. In a 500 mL three-neck round-bottom-flask, 5.5 g (0.025 mol) of PMDA was added into 80 mL of DMAC that dissolved 5.0 g (0.025 mol) of ODA. After stirring for 6 h at 5 °C, a viscous golden-green PAA solution was obtained. Then, 1.0 g nano-TiO_2 was added in PAA solution prepared by ultrasonic processing (90 HZ) with continue stirring for 3 h at 5 °C and we got PAA-TiO_2 nanocomposite solution. After that, 2.0 g TEA was added in PAA-TiO_2 solution with stirring for 1 h at 5 °C, and then it was heated to 25 °C. Finally, 30.0 mL DMAC and 360.0 mL methanol were added in the flask with stirring for 3 h at room temperature. In the whole system, the weight ratio of nano-TiO_2 to PAA and methanol to DMAC is 1:10 and 3:1, respectively. PAA-TiO_2 hybrid colloid emulsion with different ratio of methanol to DMAC was also synthesized for comparison the particle size.

Preparation of PI-TiO_2 Nanocomposite Coating. EPD was carried out by varying a number of parameters systematically while keeping the others constant under a Voltage regulator. The total process was illustrated as Chart 2. Carbon fiber bundles and graphite were selected as the anode and cathode, respectively. The anode and cathode were separated by a spacer with length of 5 cm. The electrodes were immersed in 1000 mL of the hybrid colloid emulsion and connected to the power source. The weight gain of carbon fibers was determined gravimetrically as the difference between the coated and noncoated fibers. The applied voltage was varied from 0 to 50 V in 10 V increments and the deposition time was varied from 20 to 120 s. After EPD, The coated fiber bundles were immediately withdrawn from the nanoemulsion and dried at 100 °C. Then, the PAA-TiO_2 nanocomposite coating carbon fiber were heated to 200 °C at a rate of 5 °C/min and kept for 60 min. Finally, the sample was heated to 300 °C for 60 min to obtain a PI-TiO_2 nanocomposite coating on carbon fiber. All the heat treatment process was carried out in nitrogen atmosphere and the coated fiber samples were weighed depending on various voltages.

Chart 2. Flow chart of electrochemical cell for the coating of PAA-TiO_2 hybrid colloidal particles onto carbon fiber bundle. (a) Original carbon fiber bundles, (b) anode, (c) PAA-TiO_2 hybrid colloidal particles, (d) cathode, (e) drying oven (nitrogen, 300°C), (f) PI-TiO_2 nanocomposite coating carbon fiber bundle

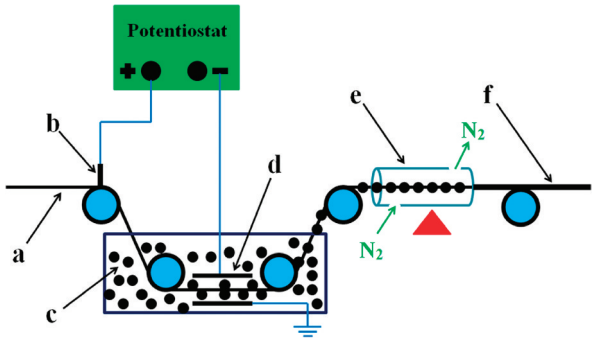

The assessment of the antiabrasion of PI-TiO_2 nanocomposite coating carbon fiber was carried out using the fiber wear rate instrument. The fiber bundles get thorough the polyurethane sponge (40 mm × 5 mm × 5 mm) at the rate of 3 m/min. Ten minutes later, ten samples were randomly chosen and weighed, and we got the average results that the coating carbon fiber showed a good

Chart 1. Formation mechanism of PAA-TiO_2 hybrid colloidal particles

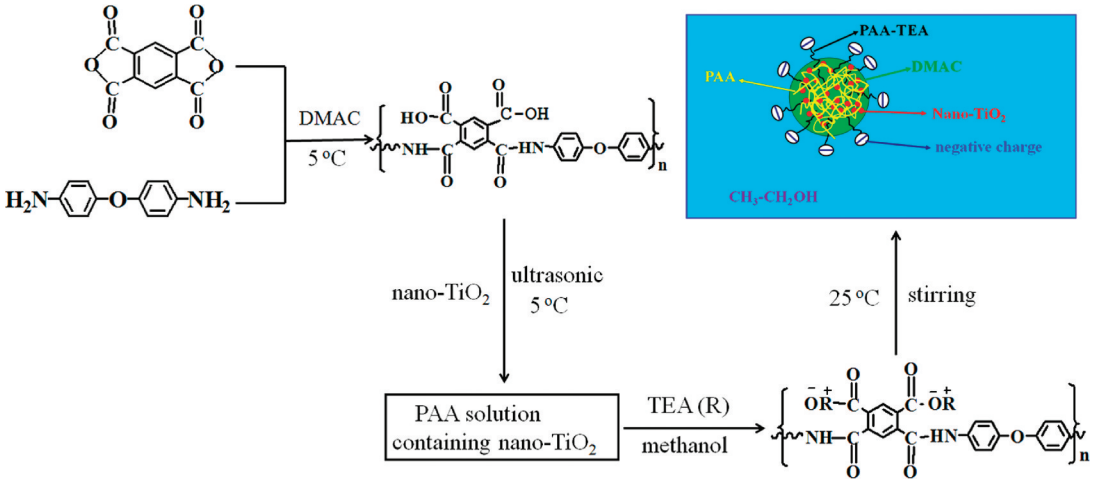

dx.doi.org/10.1021/am201239h | ACS Appl. Mater. Interfaces 2011, 3, 4744–4750

antiabrasion with little broken filament, as shown in Table 2. The mechanical strength of single fiber sample was carried out using a LLY-06E tensile testing machine (Laizhou Electron Instrument Co., Ltd. China) according to the previous research papers.[31] The cross-head speed of the tensile testing machine was 0.5 mm/min. More than 10 mm measurements within a 10% data discrete distribution were required at every gauge length of cardboard (10, 20, and 25 mm). The single fiber had no strength degradation but a little improvement, as shown in Table 3. These two table results showed preferable parameters for weaving and application in the carbon fiber sheets.

Table 2. Abrasion Rate of the Samples

sample	initial weight (g)	remain weight (g)	abrasion rate (%)
original fiber bundle	1.3000 ± 0.0006	1.2916 ± 0.0005	0.6461 ± 0.0843
PI coating fiber bundle	1.3000 ± 0.0008	1.2957 ± 0.0004	0.3307 ± 0.0921
PI-TiO_2 coating fiber bundle	1.3000 ± 0.0004	1.2971 ± 0.0007	0.2231 ± 0.0846

Table 3. Single Fiber Tensile Strengths

samples	gauge length (mm)	tensile strength (GPa)	tensile modulus (GPa)
original fiber	10	3.91 ± 0.10	230 ± 2
	20	3.89 ± 0.13	231 ± 2
	25	3.88 ± 0.15	230 ± 1
PI-TiO_2 coating fiber	10	4.11 ± 0.10	232 ± 1
	20	4.06 ± 0.09	233 ± 1
	25	4.08 ± 0.11	236 ± 2

Photodegradation Performance. The photocatalytic activities of the samples were studied by degradation experiments using methyl orange solution as model compounds. It was selected because it could be readily reduced under anaerobic conditions to produce potentially more hazardous aromatic amines. The photoreaction experiment was performed in an 800 mL rectangular vessel with a water-cooled quartz jacket. Irradiation was provided by a 500 W high-pressure mercury lamp with a major emission at 365 nm, located in the center of quartz jacket. A magnetic stirrer was equipped at the bottom of the reactor to achieve effective dispersion. Air was bubbled through the reaction solution from the bottom to ensure a constant dissolved O_2 concentration. The initial methyl orange concentration was 80 mg/L and the PI-TiO_2 coating carbon fiber sheet (10 cm × 5 cm) was used repeatedly. The temperature of reaction solution maintained at 28 ± 0.5 °C and each cycle lasted 160 min. Before the beginning of next cycle, the remaining solution was replaced by fresh methyl orange solution with 80 mg/L. The 5 mL samples were withdrawn at different intervals of time to determine the residual concentration of methyl orange by using a spectrophotometer (UV6100PC, Shanghai Analysis Company) at 462 nm. C_t and C_0 were referred to the concentration of methyl orange solution at t time and the initial time, respectively. The results presented were the mean values with a total error of less than 4%.

Characterization. The average diameter of PAA-TiO_2 hybrid colloid emulsion was measured by laser diffraction (Mastersizer Zetasizer Nano S90, Malvern, Britain). The zeta potential of the PAA-TiO_2 hybrid colloidal particles prepared was carried out to show the property and stability of the charge particles. Transmission electron microscopy (TEM) observation of PAA-TiO_2 hybrid colloidal particles was performed with a JEM-2100F (JEOL LTD, Japan) under an acceleration voltage of 200 KV. The surface morphology of PI-TiO_2 nanocomposite coating carbon fiber was observed by FE-SEM (S-4800, Hitachi High-Technologies Co, Japan). The infrared spectra of the original carbon fiber, nano-TiO_2, PI and PI-TiO_2 coating carbon fiber were recorded from 400 to 4000 cm^{-1} using a FT-IR spectroscopy (V80, Bruker Optics Co, Germany). A XRD measurement (M03XHF, Mac Science Co, Japan) with a Cu K_α radiation (λ = 1.54178 Å, 40 KV, 200 mA) were carried out to probe the structure of TiO_2 in PI-TiO_2 nanocomposite coating onto carbon fiber and scanned from 5 to 70° at step of 5°/min.

3. RESULTS AND DISCUSSION

PAA-TiO_2 Hybrid Colloid Emulsion Characterization. Colloid nanoemulsions employ better kinetic stability because of containing lots of charged particles about 20−500 nm. This property is widely utilized in chemical, cosmetic, coatings, cleaning, and pharmaceutical fields.[32] In here, the mixture of PAA-TiO_2 solution was transferred from golden-green to milky white translucent when TEA and methanol were added (Figure 1a). The Tyndall effect was appeared in PAA-TiO_2 hybrid colloidal emulsion (see Figure 1b), suggesting that there existed charged particles in colloid emulsion.

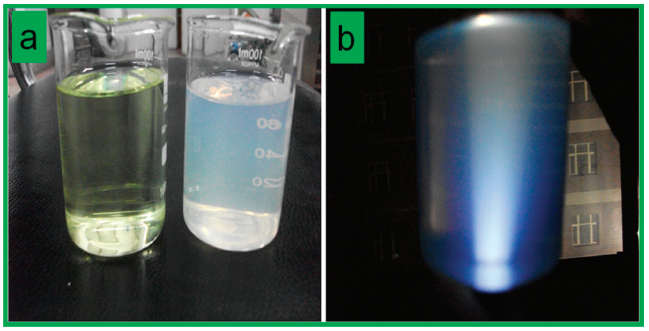

Figure 1. (a) PAA-TiO_2 solution (left, golden-green color) and PAA-TiO_2 hybrid colloidal emulsion (right, milky white), and (b) the Tyndall effect of PAA-TiO_2 hybrid colloidal emulsion.

PAA colloid emulsion particle with about 200 nm was formed at the ratio of methanol to DMAC as 3:1; a wider PAA-TiO_2 hybrid colloidal particles distribution was obtained when the nano-TiO_2 was added into (Figure 2). The nano-TiO_2 was trapped by PAA matrix in hybrid colloidal particles emulsion was observed by TEM images (Figure 3). EDX-TEM was also provided an evidence of the presence of TiO_2 in the colloidal particles (Figure 4). Furthermore, the HRTEM image of nano-TiO_2 trapped in colloidal revealed that it was anatase phase with $d_{(101)}$ = 3.53 Å and $d_{(004)}$ = 2.38 Å.

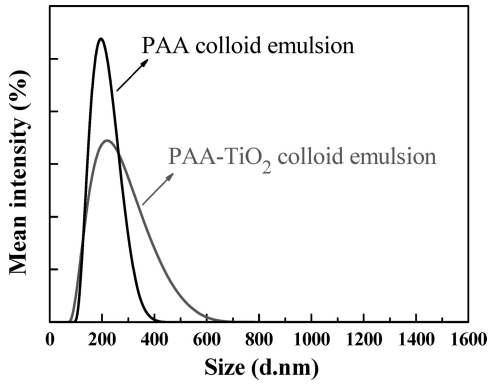

Figure 2. Size distribution of PAA colloid emulsion and PAA-TiO_2 hybrid colloid emulsion.

To compare the effect of ratio of methanol to DMAC on the particle size distribution in hybrid colloid emulsion, the average

dx.doi.org/10.1021/am201239h | ACS Appl. Mater. Interfaces 2011, 3, 4744–4750

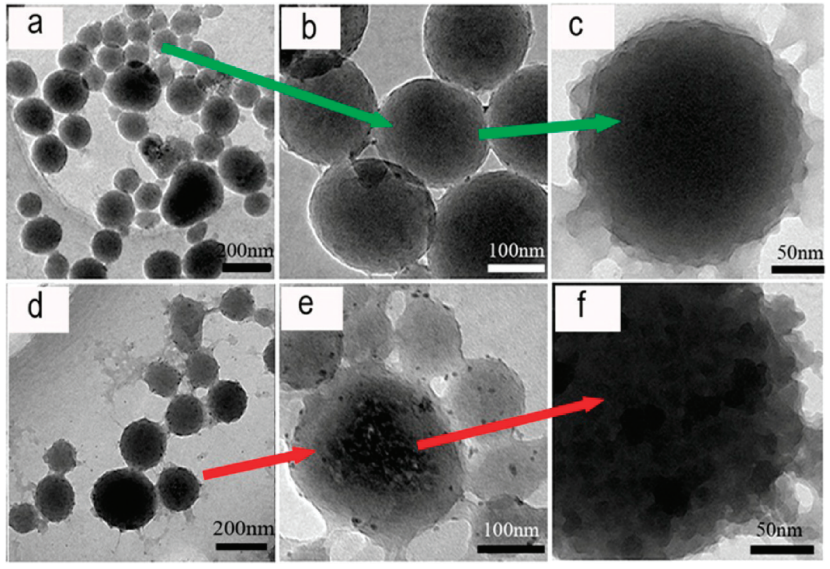

Figure 3. TEM images of (a–c) PAA colloidal particles and (d–f) PAA-TiO_2 hybrid colloidal particles.

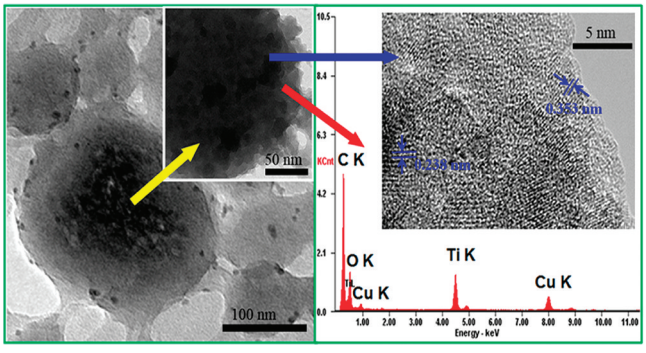

Figure 4. Elemental identification (EDX-TEM) of the colloidal particle containing nano-TiO_2 and HRTEM image of containing nano-TiO_2.

diameter of PAA-TiO_2 hybrid colloidal particles are shown in Figure 5. With the increase of precipitant (methanol), it was

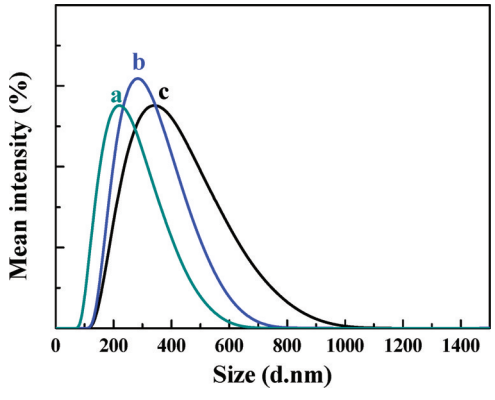

Figure 5. Size distribution of PAA-TiO_2 hybrid emulsion. The ratio of methanol to DMAC was (a) 3:1, (b) 3:1.5, and (c) 3:2, respectively.

indicated that the particles will integrate with each other and become bigger than the low methanol to DMAC ratio.

It was necessary to prepare uniform and stable PAA-TiO_2 hybrid colloidal particles in order to deposit PAA-TiO_2 hybrid colloidal particles onto carbon fiber. Here, the charged type of the colloidal particles was also investigated and the results are shown in Figure 6. The average zeta potential of the prepared

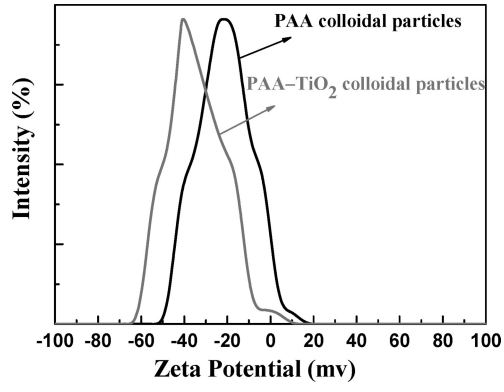

Figure 6. Zeta potential of PAA colloidal particles and PAA-TiO_2 hybrid colloidal particles.

PAA-TiO_2 hybrid colloidal particles was about −45 mV, while that of pure PAA colloidal particles was −25 mV. This indicated that the PAA-TiO_2 hybrid colloidal emulsion had better stability and the nano-TiO_2 played an important role on keeping the colloid emulsion stability.

Hybrid Colloid Emulsion Formation Mechanism and the Weight Gains of Fibers. The possible formation mechanism of PAA-TiO_2 hybrid colloidal particles was drawn in Chart 1. The hybrid emulsion particles prepared are either positively or negatively charged, depending on the charge of the dissociated end groups on the polymer molecules and of any adsorbed ions. In this work, the polymer solution contained nano-TiO_2 is obtained by dissolving the solution in DMAC. Then, a hybrid emulsion is formed by adding the PAA-TiO_2 solution into mixture of methanol and TEA. PAA-TEA salt was formed and TEA also played as anionic surfactant, so colloid consisting of PAA-TiO_2 and TEA was formed and dispersed in emulsion. The hybrid emulsion particles would migrate to the anode in an electric field because of PAA-TEA with negative charge.

dx.doi.org/10.1021/am201239h | ACS Appl. Mater. Interfaces 2011, 3, 4744–4750

The weight gain of fibers increased with applied voltage from 0 to 50 V in 120 s (see Figure 7). However, with the extending

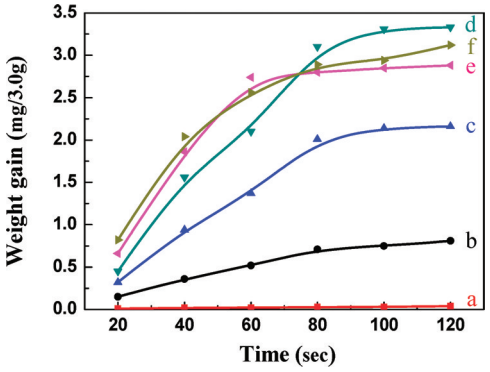

Figure 7. Weight gain of carbon fibers at different voltages of (a) 0, (b) 10, (c) 20, (d) 30, (e) 40, and (f) 50 V.

time and increasing voltage, the weight gain's velocity became slower. Additional, some gas bubble was emitted from the anode above 40 V. It suggested that electrolysis was happened on the anode at the higher voltage. Furthermore, the effect of methanol to DMAC on the weight gain of fibers was also discussed and shown in Figure 8. The weight gain of carbon

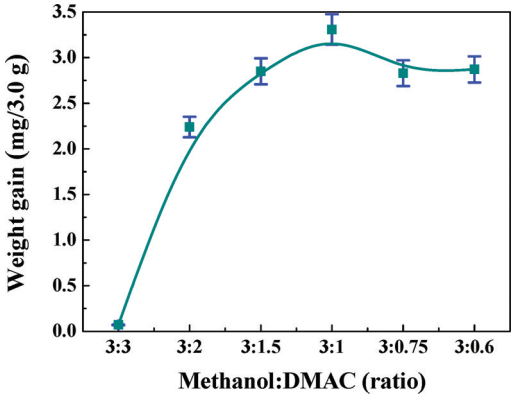

Figure 8. Dependence of the weight gain of fibers on the methanol: DMAC ratio.

fibers increased with the ratio of methanol to DMAC, and a maximum value reached at 3:1 and then leveled off. The methanol acted as a coagulant and retarded the dissolution of the coating in emulsion. When the methanol was inadequate, it would result in a higher rate of dissolution in DMAC system. As the methanol content was increased, the dissolution rate decreased, resulting in increased retention of the coatings (weight gain) on the fiber. When the methanol weight was increased to a certain value where the dissolution rate became negligible relative to the deposition rate, the weight gain of fibers would become dependent on the other deposition parameters, such as voltage and the time. So, the preferable EPD parameters voltage, methanol to DMAC, and time were listed as 30 V, 3:1, and 100 s, respectively.

FE-SEM Images. The morphology and structure of the original carbon fiber sheet and the PI-TiO_2 nanocomposite coating carbon fiber sheet were shown in Figure 9. The surface of original carbon fiber exhibited some grooves and defects formed during the carbon fiber preparation process (Figure 9a).

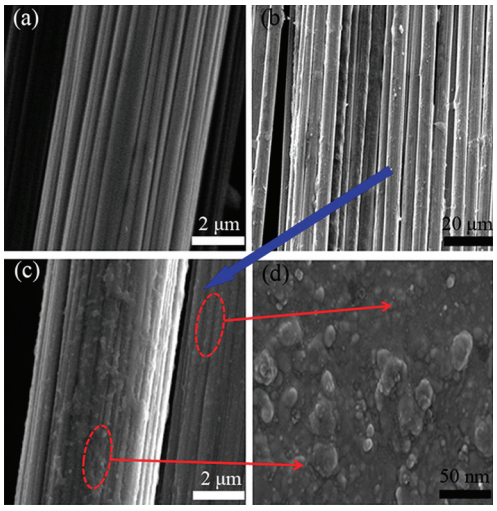

Figure 9. FE-SEM images of the samples: (a) original carbon fiber, (b–d) PI-TiO_2 nanocomposite coating carbon fiber.

During EPD process, PAA-TiO_2 hybrid colloidal particles were incorporated to form a coherent coating. After imidization, the coating was converted to polyimide with nano-TiO_2 particles impregnated. Compared with the original carbon fiber, the longitudinal striations were covered with PI-TiO_2 nanocomposite coating and became blurry and rough as displayed in images b and c in Figure 9; the detailed image is shown in Figure 9d. These roughness surfaces could provide surface area of carbon fiber and enhance the adsorption ability. Furthermore, these results indicated a favorable model that nano-TiO_2 was embedded in polyimide coating (see Figure

Figure 10. Model of PI-TiO_2 nanocomposite coating onto carbon fiber.

10). Only part of nano-TiO_2 contacted with the organic pollutants. Unlike the conventional dipping process, this EPD approach for preparation of PI-TiO_2 nanocomposite coating carbon fiber could be employed for continuous fabrication in mass production.

FT-IR Spectra Analysis. The chemical structures of the samples were characterized with a FTIR spectroscopy as shown in Figure 11. The original carbon fiber demonstrated a chemical inertness surface as displayed in Figure 11Aa. The characteristic peaks of symmetric C═O stretching and asymmetric C═O stretching of imide group were clearly visible at 1720, 1780, and 725 cm^{-1}, respectively. The assignment of the stretching of the imide ring was at 1380 cm^{-1}.[28] These mentioned peaks were the characteristic absorption of imide group and have been shown in the spectra of the entire PI and PI-TiO_2 nanocomposite coating. After the introduction of nano-TiO_2, it was observed a broad absorption band belonged to Ti–O–Ti in the range of 400–850 cm^{-1},[33] especially in the range of 400–650 cm^{-1}, shown in Figure 11Bd. Its absorbance intensity was not very strong duo to the small TiO_2 content. Meanwhile, from the FT-IR spectra of pure nano-TiO_2 (Figure 11Ab), the broad

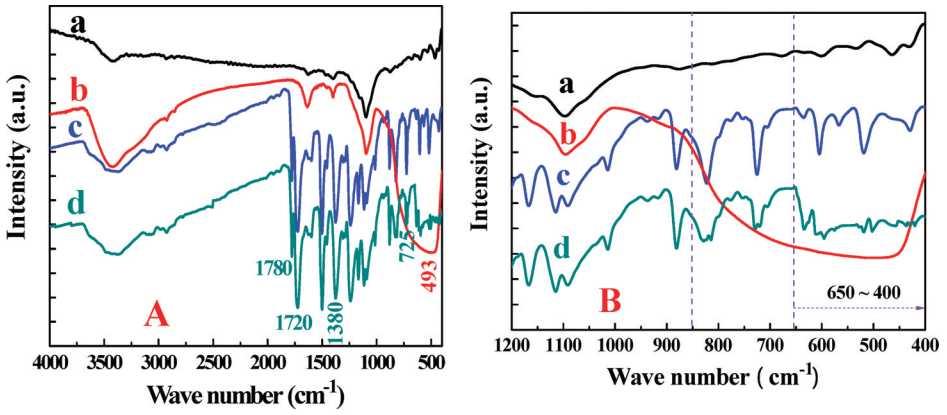

Figure 11. FT-IR spectra of the samples: (a) original carbon fiber, (b) pure nano-TiO_2, (c) pure polyimide, and (d) PI-TiO_2 nanocomposite coating carbon fiber.

absorption at 400−650 cm^{-1} result was accordance with the PI-TiO_2 nanocomposite coating. There was no absorption at 1660 and 1545 cm^{-1} for the C═O and −NH− group of PAA, which anticipated that PAA-TiO_2 hybrid colloidal particles were converted to PI-TiO_2 nanocomposite coating completely. These results indicated that the PI-TiO_2 nanocomposite coating were prepared successfully and the original carbon fiber could be coated by PI-TiO_2 nanocomposite significantly through EPD of PAA-TiO_2 hybrid colloidal particles.

Identification of the Crystal Structure of the Supported TiO_2. XRD patterns of the selected products including the original carbon fiber, pure PI coating, pure TiO_2, and PI-TiO_2 nanocomposite coating onto carbon fiber were shown in Figure 12. The diffraction angles 2θ around 25° was

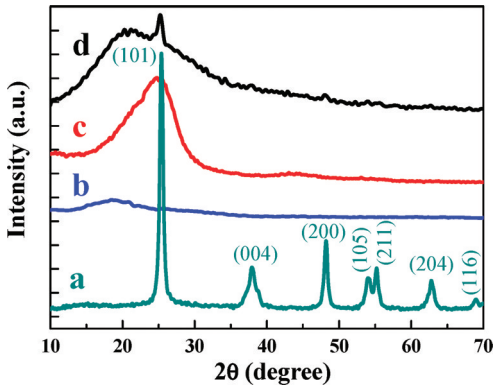

Figure 12. XRD spectra of samples: (a) pure nano-TiO_2, (b) pure PI coating onto carbon fiber, (c) carbon fiber, and (d) PI-TiO_2 nanocomposite coating onto carbon fiber.

assigned to disordered graphitic (002) in original carbon fiber,[34] as shown in Figure 12c. Pure PI coating displayed a broad hump centered at 2θ = 19°, originating from amorphous phase of aromatic polyimide. There were no peaks founded at 27.4, 36.1, and 41.2° that belong to the diffraction peaks of (110), (101), and (111) of rutile. In addition, after introduction of TiO_2, PI-TiO_2 nanocomposite coating showed three major characteristic diffraction peaks at (101), (004), (200) plane of the anatase phase TiO_2, corresponding to the *d*-spacing of nearly 3.53, 2.38, and 1.89 Å, respectively, which was a good agreement with the HETEM results in Figure 4. Furthermore, these results provided good evidence that the nano-TiO_2 was embedded on PI coating carbon fiber.

Photodegradation Performance of PI-TiO_2 Nanocomposite Coating Carbon Fiber. TiO_2 nanomaterials normally have electronic band gaps larger than 3.0 eV and high absorption in the UV region. It is most used for photodegradation of various pollutants and the photocatalytic reaction mechanisms are widely studied,[35] according to the following scheme

$$TiO_2 + hv \longrightarrow h^+ + e^-$$
$$h^+ + OH^- \longrightarrow \cdot OH$$
$$h^+ + H_2O \longrightarrow \cdot OH + H^+$$
$$e^- + O_2 \longrightarrow O_2^-$$
$$O_2^- + H^+ \longrightarrow HO_2^-$$
$$HO_2^- + H^+ \longrightarrow H_2O_2$$
$$\cdot OH + \text{methyl orange} \longrightarrow CO_2 + H_2O$$

Irradiating UV light with wavelength around 380 nm on TiO_2 surface creates positive holes (h^+) and electron (e^-) pairs that act as powerful oxidizing and reducing agents, respectively. These charge carriers would then lead to the generation of highly reactive oxidants, such as hydroxyl radicals (•OH), superoxide anions (O_2^-), hydrogen peroxide (H_2O_2) and other reactive oxygen species. As a result of oxidative and reductive reactions it further involves in the decompositions of organic compounds (dyes) adsorbed on the TiO_2 surface.

The photocatalytic degradation of methyl orange was shown in Figure 13. PI coating carbon fiber had no catalytic activity in the degradation of methyl orange under UV irradiation. Methyl

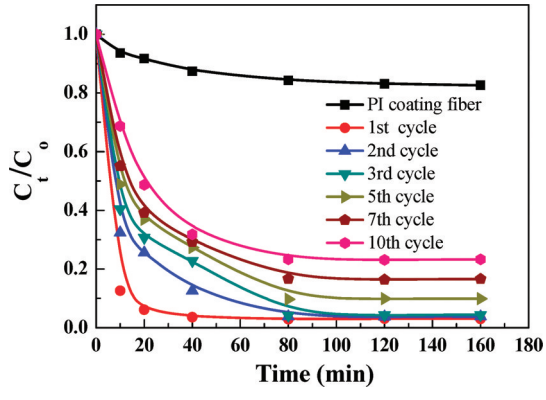

Figure 13. Photocatalytic degradation properties of the samples.

dx.doi.org/10.1021/am201239h | ACS Appl. Mater. Interfaces 2011, 3, 4744–4750

orange removal without TiO_2 was also carried out to observe the UV photolysis effect of methyl orange. It was observed that methyl orange was quite stable when it was irradiated under UV without TiO_2, only 13% methyl orange decrease, suggesting that the disappearance of methyl orange caused by UV irradiation was negligible. It could be seen that methyl orange was removed from water rapidly by the modified carbon fiber sheet for the first cycle. With the cycle times increasing, the removal efficiency was decreasing. But, it still remained nearly 70% removal capacity of methyl orange after ten cycles. This result suggested that PI-TiO_2 nanocomposite coating carbon fiber sheet sample was recycled and maintained high activity relatively. Furthermore, the PI-TiO_2 nanocomposite coating carbon fiber sheet was potentially employable for continuous photodegradation process for larger area water pollution.

4. CONCLUSION

A facile and efficient approach to prepared PAA-TiO_2 hybrid colloid emulsion and PI-TiO_2 nanocomposite coating has been developed successfully. PAA-TiO_2 hybrid colloidal particles as low as 200 nm have been obtained. Experimental results indicated that small amount of nano-TiO_2 would be dispersed in PAA colloidal particles effectively. By using EPD, the PI-TiO_2 nanocomposite coating could be fabricated onto carbon fiber. This nanocomposite coating carbon fiber was recoverable and durable and played a significant role in facilitating the treatment of methyl orange. Furthermore, this novel nanocomposite coating method may provide a new idea for carbon fiber application in functionality materials fields, such as antiaging, self-cleaning, and antibacterial.

AUTHOR INFORMATION

Corresponding Author

*E-mail: chunxl@sxicc.ac.cn. Tel/Fax: +86-351-4166215.

ACKNOWLEDGMENTS

The authors acknowledge financial supports for this research work from the National Natural Science Foundation of China (Grant 50602045), the Graduate Innovation Foundation of Shanxi province, China (Grant 20113124), and the Technology Innovation Foundation of Graduate University of Chinese Academy of Sciences.

REFERENCES

(1) Gratzel, M. *Nature* **2001**, *414*, 338−344.
(2) Kamat, P. V. *Chem. Rev.* **1993**, *93*, 267−300.
(3) Fujishima, A.; Honda, K. *Nature* **1972**, *238*, 37−38.
(4) Feldman, Y.; Wasserman, E.; Srolovitch, D. J.; Tenne, R. *Science* **1995**, *267*, 222−225.
(5) Shi, J. W.; Zheng, J. T.; Wu, P.; Ji, X. J. *Catal. Commun.* **2008**, *9*, 1846−1850.
(6) Fabian, S. -G.; Amelia, M. -A.; Tascón, J. M. D. *Carbon* **2004**, *42*, 1419−1426.
(7) Huang, Z. -H.; Kang, F. Y.; Huang, W. L.; Yang, J. -B.; Liang, K. -M.; Cui, M. -L.; Cheng, Z. Y. *J. Colloid Interface Sci.* **2002**, *249*, 453−457.
(8) Paiva, M. C.; Bernardo, C. A.; Nardin, M. *Carbon* **2000**, *38*, 1323−1337.
(9) Landry, C. C.; Barron, A. R. *Carbon* **1995**, *33*, 381−387.
(10) Naito, K.; Yang, J.-M.; Xu, Y. B.; Kagawa, Y. *Carbon* **2010**, *48*, 1849−1857.
(11) Chen, P.; Gu, L.; Xue, X. D.; Li, M. J.; Cao, X. B. *Chem. Commun.* **2010**, *46*, 5906−5908.
(12) Zeng, J.; Xu, J. C. *J. Alloys Compd.* **2010**, *493*, L39−L41.
(13) Cao, M. S.; Song, W. L.; Hou, Z. L.; Wen, B.; Yuan, J. *Carbon* **2010**, *48*, 788−796.
(14) Das, N. C.; Khastgir, D.; Chaki, T. K.; Chakraborty, A. *Compos., Part A: Appl. Sci.* **2000**, *31*, 1069−1081.
(15) Lin, Y. R.; Ehlert, G.; Sodano, H. A. *Adv. Funct. Mater.* **2009**, *19*, 2654−2660.
(16) Zhao, F.; Huang, Y. D. *J. Mater. Chem.* **2011**, *21*, 3695−3703.
(17) Ryu, S.-K.; Park, B.-J.; Park, S.-J. *J. Colloid Interface Sci.* **1999**, *215*, 167−169.
(18) Ganesan, Y.; Peng, C.; Lu, Y.; Loya, P. E.; Moloney, P.; Barrera, E.; Yakobson, B. I.; Tour, J. M.; Ballarini, R.; Lou, J. *ACS Appl. Mater. Interfaces* **2011**, *3*, 129−134.
(19) Sanchez, C.; Belleville, P.; Popall, M.; Nicole, L. *Chem. Soc. Rev.* **2011**, *40*, 696−753.
(20) Brun, N.; Ungureanu, S.; Deleuze, H.; Backov, R. *Chem. Soc. Rev.* **2011**, *40*, 771−788.
(21) Thompson, R. B.; Ginzburg, V. V.; Matsen, M. W.; Balazs, A. C. *Science* **2001**, *292*, 2469−2472.
(22) Aminian, M. K.; Taghavinia, N.; Irajizad, A.; Mahdavi, S. M. *J. Phys. Chem. C* **2007**, *111*, 9794−9798.
(23) Hasegawa, M.; Horie, K. *Prog. Polym. Sci.* **2001**, *26*, 259−335.
(24) Ge, J. J.; Zhang, D.; Li, Q.; Hou, H. Q.; Graham, M. J.; Dai, L. M.; Harris, F. W.; Cheng, S. Z. D. *J. Am. Chem. Soc.* **2005**, *127*, 9984−9985.
(25) Tyan, H.-L.; Liu, Y.-C.; Wei, K.-H. *Polymer* **1999**, *40*, 4877−4886.
(26) Nandi, M.; Conklin, J. A.; Salvati, L.; Sen, A. *Chem. Mater.* **1991**, *3*, 201−206.
(27) Chiang, P.-C.; Whang, W.-T. *Polymer* **2003**, *44*, 2249−2254.
(28) Liu, J.-G.; Nakamura, Y.; Ogura, T.; Shibasaki, Y.; Ando, S.; Ueda, M. *Chem. Mater.* **2007**, *20*, 273−281.
(29) Wu, D. C.; Shen, L.; Low, J. E.; Wong, S. Y.; Li, X.; Tjiu, W. C.; Liu, Y.; He, C. B. *Polymer* **2010**, *51*, 2155−2160.
(30) Kim, S.-K.; Lee, H.; Tanaka, H.; Weiss, P. S. *Langmuir* **2008**, *24*, 12936−12942.
(31) Zhao, F.; Huang, Y. *J. Mater. Chem.* **2011**, *21*, 2867−2870.
(32) Solè, I.; Maestro, A.; González, C.; Solans, C.; Gutiérrez, J. M. *Langmuir* **2006**, *22*, 8326−8332.
(33) Sui, R. H.; Rizkalla, A. S.; Charpentier, P. A. *J. Phys. Chem. B* **2006**, *110*, 16212−16218.
(34) Park, S.-J.; Seo, M.-K.; Lee, Y.-S. *Carbon* **2003**, *41*, 723−730.
(35) Chen, X.; Mao, S. S. *Chem. Rev.* **2007**, *107*, 2891−2959.